Journal of ELECTRONIC MATERIALS, Vol. 47, No. 2, 2018
https://doi.org/10.1007/s11664-017-5986-7

TOPICAL COLLECTION: 59TH ELECTRONIC MATERIALS CONFERENCE 2017

Shape Evolution of Highly Lattice-Mismatched InN/InGaN Nanowire Heterostructures

LIFAN YAN,[1,3,4] ARNAB HAZARI,[1,2] PALLAB BHATTACHARYA,[2] and JOANNA M. MILLUNCHICK[1,5]

1.—Center for Photonics and Multiscale Nanomaterials, University of Michigan, Ann Arbor, MI 48109, USA. 2.—Department of Material Science and Engineering, University of Michigan, Ann Arbor, MI 48109, USA. 3.—Department of Electrical Engineering and Computer Science, University of Michigan, Ann Arbor, MI 48109, USA. 4.—e-mail: ylifan@umich.edu. 5.—e-mail: joannamm@umich.edu

We have investigated the structure and shape of GaN-based nanowires grown on (001) Si substrates for optoelectronic device applications. The nanowire heterostructures contained InN disks and $In_{0.4}Ga_{0.6}N$ barrier layers in the active region. The resulting nanowire array comprised two differently shaped nanowires: shorter pencil-like nanowires and longer bead-like nanowires. The two different nanowire shapes evolve due to a variation in the In incorporation rate, which was faster for the bead-like nanowires. Both types of nanowires exhibited evidence of significant migration of both Ga and In during growth. Ga tended to diffuse away and down along the sidewalls, resulting in a Ga-rich shell for all nanowires. Despite the complex structure and great variability in the In composition, the optical properties of the nanowire arrays were very good, with strong luminescence peaking at ~ 1.63 μm.

Key words: InGaN, InN, nanowires, infrared, photoluminescence, STEM

INTRODUCTION

InGaN nanowire heterostructures have been proposed for use in optoelectronic devices, such as light-emitting diodes,[1–3] lasers,[4,5] and sensors,[6] due to the high tunability of their bandgap, which can range from the deep-ultraviolet to infrared wavelength regime depending on the In composition.[5,7,8] These nanowire structures also provide structural advantages, as they can be grown directly on (001) Si wafer, making them suitable for potential integration, and have been shown to effectively relax lattice mismatch strain at low In compositions.[5,9]

The shape of such nanowires can be altered by tuning the growth conditions and In composition. For low In concentrations, nanowire heterostructure growth occurs axially on the basal plane, resulting in disc-in-nanowire heterostructures.[10] As the In concentration increases, the lattice mismatch also increases such that the growth mode of the In-rich region may transition from layer-by-layer to three-dimensional island nucleation within the nanowire,[11] analogous to Stranski–Krastanov growth of quantum dots in planar epitaxial systems.[12] Decreasing the substrate temperature has been shown to promote In incorporation and lateral growth of nanowires.[13] Reducing the growth temperature while simultaneously increasing the In composition shifts the primary growth directions away from the basal plane to pyramidal planes;[14,15] For example, growth of $In_{0.4}Ga_{0.6}N$ on top of GaN nanowires results in such a drastic increase in diameter that the nanowires coalesce.[16] It has been shown that pure InN nanowires also increase in diameter during growth, resulting in inverted pyramids or pinhead structures.[17–19]

Details about the structure of highly lattice-mismatched InGaN nanowire heterostructures, where there is variation in the In composition along the length of the nanowire, have not been reported. However, it is expected that the interaction of composition- and temperature-induced morphological changes and strain relaxation will have a strong

(Received June 26, 2017; accepted November 20, 2017; published online December 1, 2017)

impact on the final shape and compositional distribution across the resulting nanowire arrays. To investigate this phenomenon more closely, multiple heterostructure nanowires were examined using high-resolution transmission electron microscopy (TEM). Temperature-dependent photoluminescence from the nanowires was also recorded.

EXPERIMENTAL PROCEDURES

To understand the behavior of In-rich InGaN nanowire heterostructures, two nanowire samples were grown by plasma-assisted molecular beam epitaxy (PAMBE) using growth parameters similar to those of prior work.[5] Both nanowire heterostructures were grown on *n*-type (001) Si substrates without treatment before going into the MBE chamber. In both samples, a 260-nm-thick *n*-GaN stem was grown under nitrogen-rich conditions at substrate temperature of 819°C with Ga flux of 1.56×10^{-8} kPa. The substrate stage rotated at 3 rpm during growth. A graded $In_xGa_{1-x}N$ buffer layer, with intended composition in the range of $0 \le x \le 0.4$, was grown by lowering the substrate temperature from 819°C to 631°C in 10 steps, while holding the Ga and In fluxes constant at 1.47×10^{-8} kPa and 5.73×10^{-9} kPa, respectively. During growth of the active region consisting of alternating InN disks and $In_{0.4}Ga_{0.6}N$ barriers, the substrate temperature was lowered to 433°C while the In flux was kept fixed at 5.33×10^{-9} kPa. The 12-nm-thick barriers were grown by exposing the substrate to an additional Ga flux of 1.8×10^{-9} kPa. Sample A had four InN disks of 6 nm thickness in the active region and a 150-nm-thick *p*-GaN capping layer on top grown at 819°C with Ga flux of 1.28×10^{-8} kPa. A schematic of this intended structure is shown in Fig. 1a. Sample B was grown with six alternating InN disks and $In_{0.4}Ga_{0.6}N$ barriers of the same respective thicknesses in the active region, while the *p*-GaN capping layer was omitted.

TEM samples were prepared either by removing the nanowires from the substrate and dispersing them with water on a lacy carbon film mesh Cu TEM grid, or by focused ion beam (FIB) milling. In the latter case, the final step in polishing the TEM sample was conducted at low voltage (2 kV) and current (4 pA) to avoid Ga-induced damage. Transmission electron micrographs and energy-dispersive x-ray spectroscopy (EDS) data were collected using a JEOL JEM 2100 scanning transmission electron microscope (STEM) with CEOS probe corrector and attached EDAX 100 mm^2 silicon drift detector (SSD). The microscope was operated in STEM mode with the lens settings defining probe size of $\sim$ 0.15 nm for high-angle annular dark-field (HAADF) imaging and a detector collection inner angle of $\sim$ 75 mrad. EDS mapping data were collected with Ga K peak at 9.24 kV and In L peak at 3.28 kV. For the EDS line profile, the distance between each data point was set at 2 nm.

RESULTS AND DISCUSSION

Figure 1b shows a scanning electron micrograph of the GaN/InGaN/InN nanowire heterostructure from sample A. The average length of the nanowires in this sample was $\sim$ 500 nm, though the length varied from wire to wire. Instead of presenting prismatic shape, as reported for nanowire heterostructures with lower In composition,[20] these nanowires exhibited two distinct morphologies: a pointed pencil-shape and a rounded polyhedral bead-like shape. One representative nanowire for each morphologies is indicated in Fig. 1b. The pencil-like wires, which constituted $\sim$ 60% of the array, sometimes exhibited periodic spike-like protrusions in the In-rich regions, in agreement with reports on $In_{0.4}Ga_{0.6}N$ disk-in-nanowire structures.[21] The bead-like wires, on the other hand, comprised highly faceted polyhedra. As seen from the image, the polyhedral bead-shape nanowires were much taller than the pencil-shaped nanowires. The average height of the pencil-shape nanowires was$\sim$ 400 nm, while the polyhedral bead-shape nanowires were usually $\sim$ 600 nm long. The size of the beads increased along the growth; lower beads had diameter of $\sim$ 50 nm, while the topmost beads had diameters on the order of $\sim$ 100 nm. Sample B exhibited a similar distribution of nanowire shapes, except that the average height of the nanowires was $\sim$ 700 nm, because of the additional layers in the active region.

Figure 2a shows a HAADF image of a pair of pencil-shaped nanowires dispersed on a Cu grid from sample A, along with the EDS mapping results for the Ga (Fig. 2b) and In (Fig. 2c) distributions within them. These images clearly show that a Ga-rich shell wraps around each In-rich region. Figure 2d shows the line profile of the In composition for the line indicated in Fig. 2a. The composition was calculated based on the assumption that the total amount of group III elements (In and Ga) equals the amount of group V element (N), while the In composition was obtained by dividing the total number of In counts by the total number of counts for the group III elements. Four In-rich regions can be clearly identified in this nanowire. The composition of the In-rich regions increased with increasing thickness, from $\sim$ 60% in the bottommost layer to $\sim$ 80% for the topmost layer. Similarly, the composition of the barrier layers increased from $\sim$ 20% for the layer just below the bottommost layer to $\sim$ 30% for the layer above the topmost layer, again confirming strong In segregation. The ratio of the InN disk thickness to barrier layer thickness had an average value of 0.5 ± 0.2, in reasonable agreement with the intended ratio of 0.5 despite the large variation.

Figure 3a shows a HAADF STEM image of a representative bead-like nanowire in sample B dispersed on a TEM grid. In this nanowire, five polyhedral beads were visible, and the active region had total length of $\sim$ 300 nm. The bead diameter

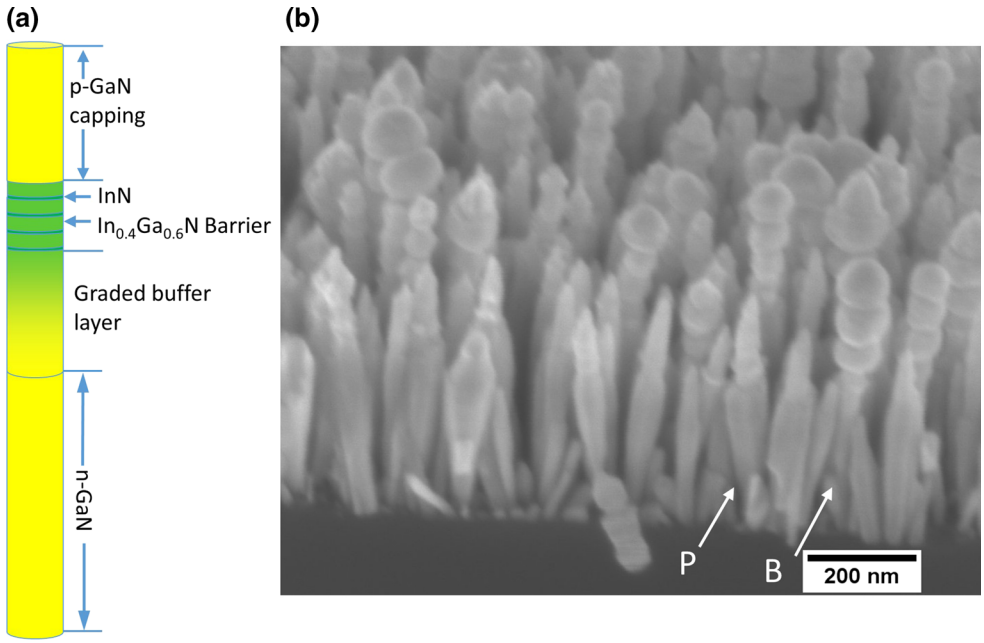

Fig. 1. (a) Schematic of intended InN/$In_{0.4}Ga_{0.6}N$ disk in nanowire heterostructure. (b) SEM image of nanowire morphology for sample A at 52° tilt. Examples of pencil-shaped (P) and bead-shaped (B) nanowires are indicated.

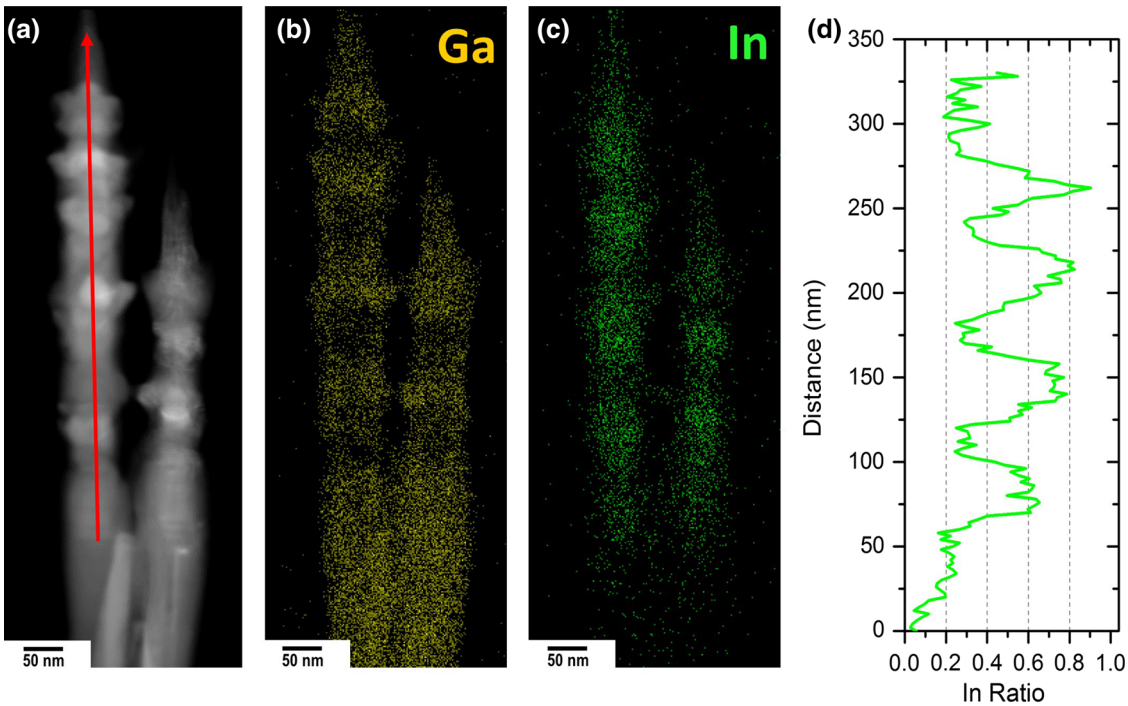

Fig. 2. (a) HAADF image of a pair of pencil-shaped nanowires from sample A. EDS mapping of these wires indicating the distribution of (b) Ga and (c) In. (d) In ratio along the line indicated in (a).

increased from ~ 50 nm to ~ 100 nm along the nanowire, being comparable to the diameters observed in sample A. The two bottommost beads were fairly narrow and largely obscured by a GaN shell, suggesting that a great deal of Ga migration occurred along the sidewalls during growth of the barrier layers. In fact, it is likely that the sixth bead, the first one to be deposited, was entirely obscured by the GaN shell. As seen in the image, the brighter-contrast In-rich regions form the "pinhead" structure frequently observed for higher-In-concentration layers on GaN nanowires.[19] Figure 3b shows a

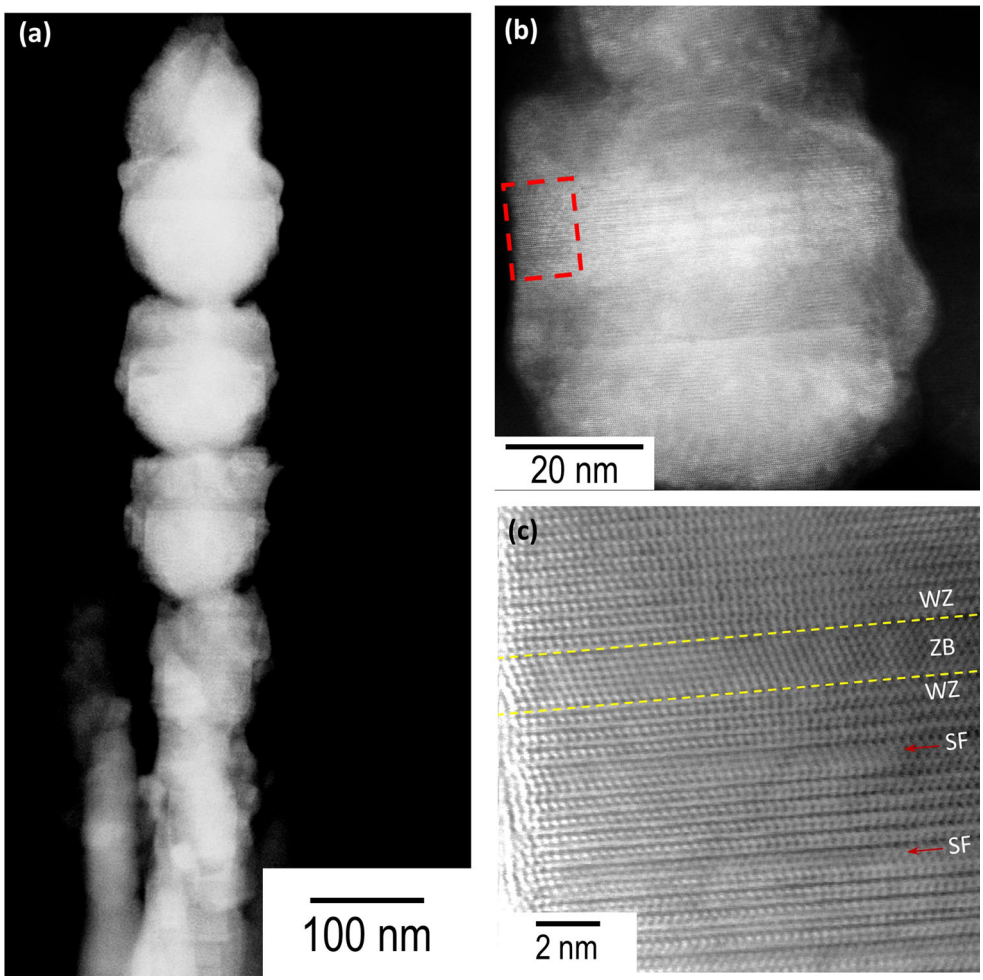

Fig. 3. (a) HAADF STEM micrograph of typical bead-like nanowire in sample B. (b) Higher-resolution HAADF STEM image of a single bead (c) ABF image of region indicated in (b) showing multiple stacking faults (SF), and regions of wurtzite (WZ) and zincblende (ZB) crystal structures.

higher-magnification HAADF image of a single bead, revealing that the Ga-rich barrier layer exhibited contrast modulation parallel to the growth surface. This contrast variation is often observed in only Ga-rich barrier layers in bead-like nanowires. The high-resolution annular bright-field (ABF) image in Fig. 3c clearly shows that this contrast resulted from stacking faults as opposed to variations in In composition. In this case, the brighter regions correspond to zincblende phase, which has slightly higher density, while darker regions correspond to wurtzite phase.

Figure 4a–d presents EDS data for the nanowire shown in Fig. 3a. Figure 4a shows a STEM image of the EDS data mapping area. The spatial distributions of Ga-rich and In-rich regions are shown in Fig. 4b and c, respectively. Figure 4d shows the line profile of the In composition calculated using the same method as for Fig. 2e. A Ga shell is again apparent from the EDS results, being thicker for the lower beads. Similar to the pencil-like nanowires, the In composition was $\sim 65\%$ for the lowest bead, and increased monotonically with each bead, culminating in a nominal composition of 90% for the uppermost bead. The difference is that the In-rich layers in the bead-like nanowires were significantly thicker, suggesting that In was incorporated at higher rates in these than in the pencil-like nanowires. This is borne out by the fact that the ratio of the InN layer thickness to barrier layer thickness was 1.7 ± 0.4, more than three times the intended value of 0.5. The Ga-rich barriers for these nanowires also increased in In concentration along the axis of the nanowire, although the composition was somewhat higher than in the pencil-like wires, starting at 30% at the first barrier and increasing to 50% between the last bead and the apex of the wire. The nanowire tip was In rich in the center, with a thin GaN shell on its topmost surface. These data together again show that there was a strong driving force for In segregation along the axis of the nanowire, and migration of Ga along the sidewalls, in agreement with other reports.[19]

The development of two different nanowire morphologies was unexpected. A possible cause for this difference in nanowire length may be shadowing,

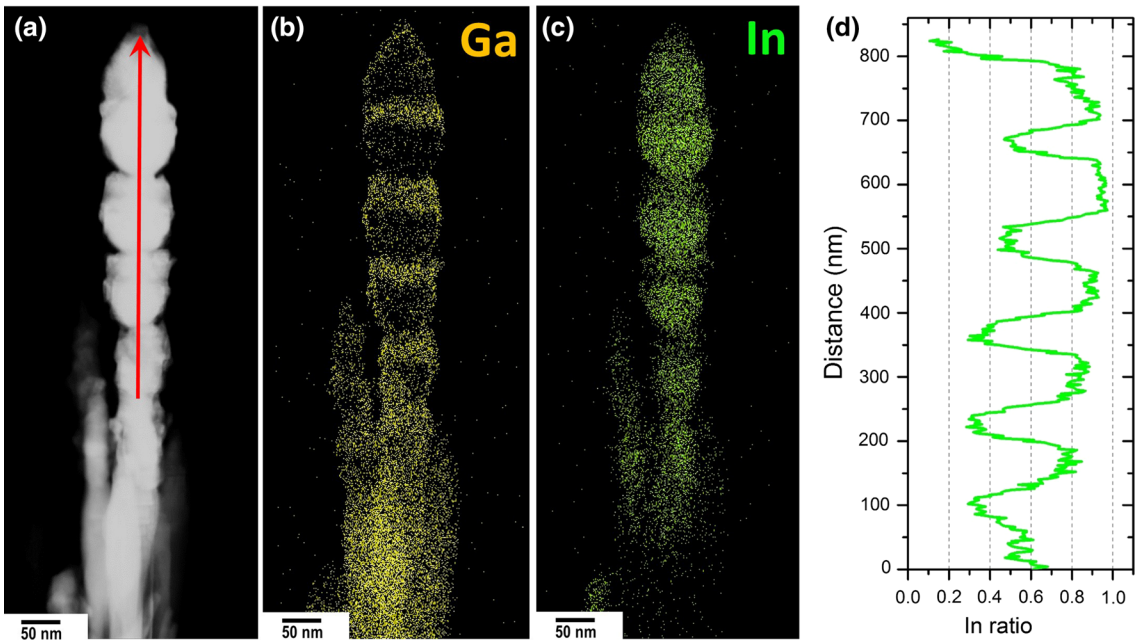

Fig. 4. (a) HAADF image of bead-shaped nanowire from sample B. EDS mapping of this wire indicating the distribution of (b) Ga and (c) In. (d) In ratio along the line indicated in (a).

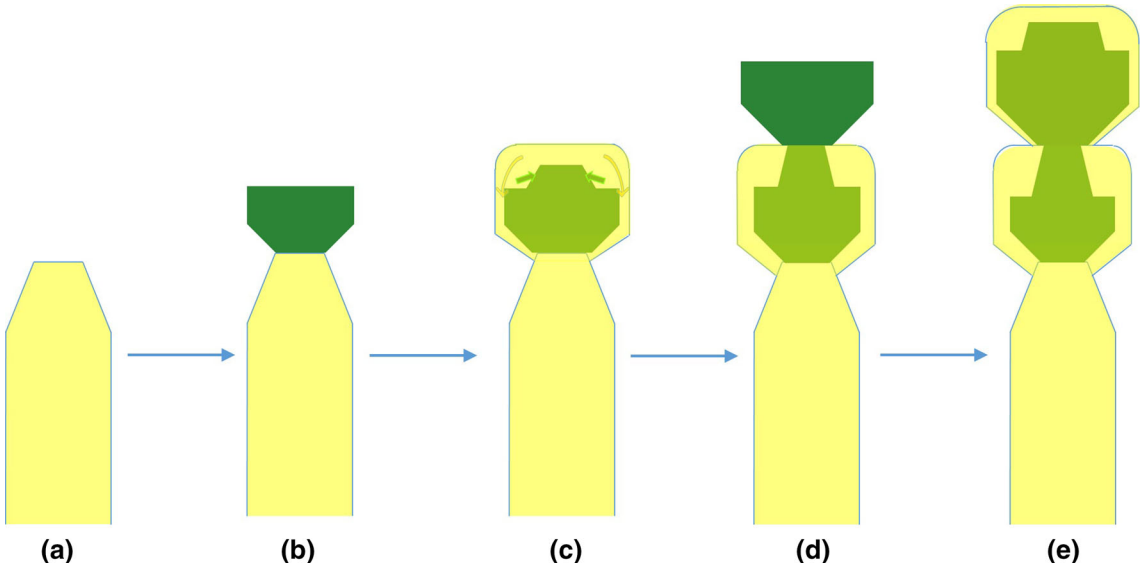

Fig. 5. Schematic showing how the bead shape nanowire develops: (a) before deposition of active region, (b) deposition of first InN layer, (c) deposition of first barrier layer, where the arrow indicates indium segregation inwards while Ga migrates outwards, (d) after deposition of second InN layer, and (e) after deposition of second barrier layer.

whereby taller nanowires block any nonnormal incident flux from reaching shorter ones,[22] although this effect would be removed in the case of substrate rotation. It is interesting to note that, in addition to the length, the total amount of In in the bead-like wires was larger, especially in the barrier layers (Figs. 2d and 4d). These observations suggest higher In incorporation in the bead-like nanowires. Differences in the incorporation of In may be related to the polarity of the crystal structure in the nanowire; For instance, Zhang et al.[19] reported that InGaN layers only form on top of GaN nanowires that are entirely N-polar, and that nanowires having Ga-polar cores did not exhibit any In incorporation. The polarity of the initial GaN nanowires examined here could not be easily determined in these nanowires using converged-beam diffraction, due to the core–shell structure and the highly lattice mismatch that develops as more InN–InGaN barrier layer pairs are deposited. Experiments are

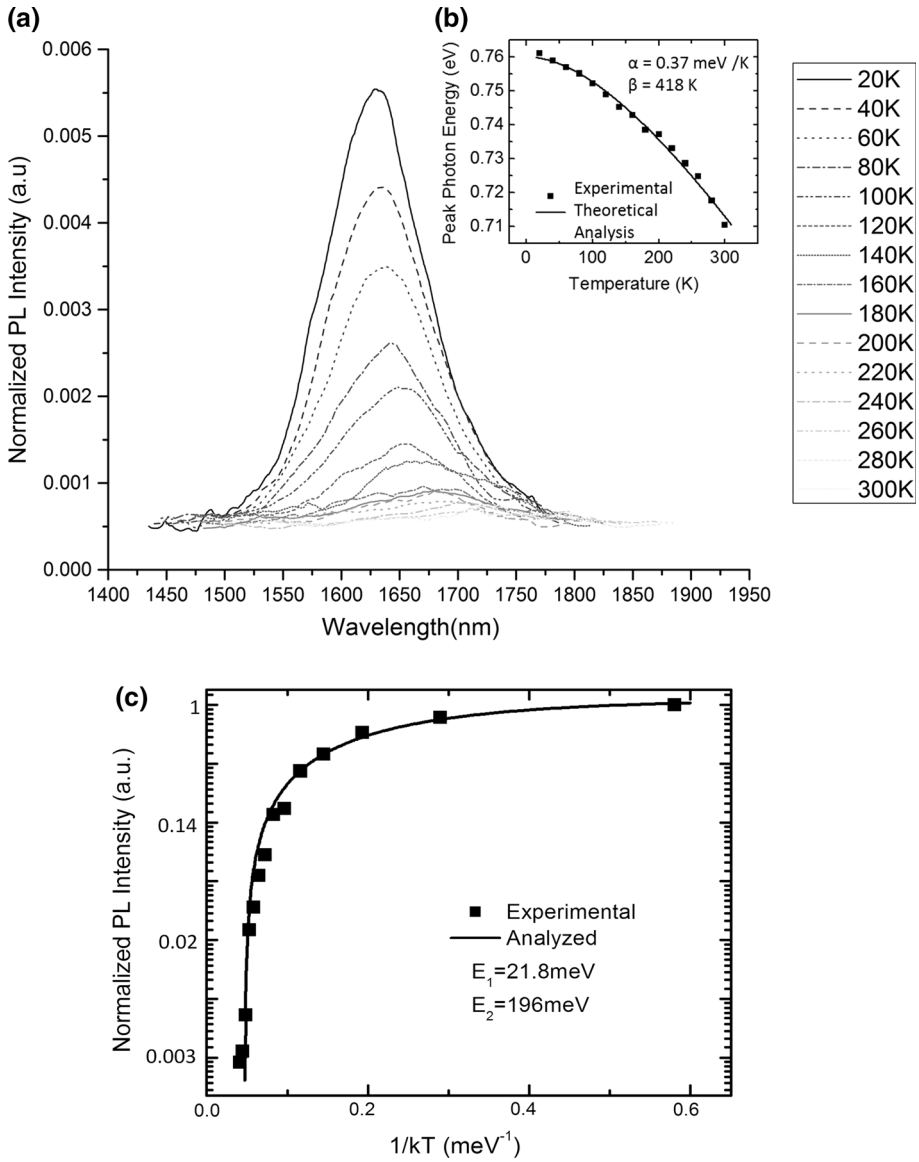

Fig. 6. PL results of sample A. Low-temperature to room-temperature (a) PL intensity and (b) peak photon energy, both experimental data points and fitted curve. (c) Normalized PL intensity (a.u.) versus $1/kT$ (meV^{-1}).

underway to validate this hypothesis. However, Wang et al. found that Ga-polar nanowires have pointed tops, which is consistent with the observed crystal shape of the shorter nanowires.[16]

Variation in the In incorporation rate could also explain the development of the two morphologies. The growth front of the InGaN graded layer is prismatic. Upon deposition of InN, the width of the nanowire initially increases until a new equilibrium width is reached, resulting in a pinhead structure. Deposition of the Ga-rich InGaN barrier layer again proceeds prismatically, with a narrower basal plane region. At the same time, In tends to migrate towards the center and up the nanowire, and Ga tends to migrate away and down along the sidewalls, thus forming a Ga-rich shell. This process repeats for each InN–InGaN pair, resulting in a bead-like structure with a thicker Ga-rich shell towards the lower portion of the active region, and larger In-rich beads towards the top of the active region (Fig. 5). We propose that the pencil-like structure develops in the same way, except that the lower In incorporation rate results in thinner In-rich layers such that the full pinhead structure does not form, resulting instead in an inverted pyramid shape. As the InGaN barrier layers are deposited, the In again migrates up and towards the center of the wire, with Ga migrating away and down. The spiky protrusions arise from the misorientation of the GaN shell in response to stacking faults in the In-rich layer.[23]

Despite the complex composition profiles observed in these structures, the optical properties were surprisingly robust. Temperature-dependent photoluminescence (PL) measurements were performed by placing the nanowire sample (sample A) in a He cryostat and exciting at 325 nm using a He-Cd laser. The luminescence was analyzed using an Acton spectrometer with resolution of 0.03 nm, and detected by a liquid-nitrogen-cooled Ge detector. The temperature-dependent PL spectra measured at excitation intensity of 50 kW/cm^2 are shown in Fig. 6a. The emission peak at room temperature was found at $\sim$ 0.71 eV (1.75 μm). The variation of the PL emission peak energy with temperature (Fig. 6b) was analyzed using the Varshni equation[24] with parameter values of α = 0.37 meV/K and β = 418 K. The temperature dependence of the peak emission energy (shown in the inset) did not exhibit any S-type behavior, suggesting that the emission was not influenced by compositional inhomogeneities.[25] The measured variation of the integrated PL intensity with temperature is depicted in Fig. 6b. The overall temperature dependence can be analyzed using activation energies of E_1 = 21.8 meV and E_2 = 196.0 meV. The value of E_1 is in good agreement with the X_A exciton binding energy, and the quenching of luminescence represents deactivation of the free exciton.[26] The value of E_2 is much smaller than the band offset under flat-band conditions. However, due to the presence of the polarization field, the effective barrier to electron escape from the ground state by field-assisted emission or tunneling could be much smaller, comparable to 196 meV. These electrons can then recombine nonradiatively in the barriers or other regions of the heterostructure. Indeed, deep-level traps have been identified in GaN nanowires.[3]

CONCLUSIONS

This paper shows that growth of highly lattice-mismatched InN-InGaN heterostructure nanowires results in two distinct morphologies: shorter sharp-tipped pencils and longer rounded beads. The bead-like wires tended to be longer overall and have thicker In-rich layers than the pencil-like wires. The composition of the In-rich regions in both types was nominally the same, but the In composition of the barrier layers was higher for the bead-like nanowires. Thus, this dual morphology may be explained by wire-to-wire variation in the In incorporation rate, possibly due to variation in the polarity of the underlying crystal structure. Both types of wires showed evidence of significant In segregation up and towards the center of the wire, and Ga migration away and down along the wire sidewalls. Despite the complex morphologies, the optical properties of these structures were very good, with strong emission at energies consistent with homogeneous InN layers.

ACKNOWLEDGEMENTS

The work was supported by the National Science Foundation, MRSEC Program, under Grant DMR-1120923 and financially by the University of Michigan College of Engineering. The authors acknowledge Dr. K. Sun and help provided by the Michigan Center for Materials Characterization through use of instruments and staff assistance.

REFERENCES

1. S. Nakamura, T. Mukai, and M. Senoh, *Appl. Phys. Lett.* 64, 1687 (1994).
2. Y. Taniyasu, M. Kasu, and T. Makimoto, *Nature* 441, 325 (2006).
3. S. Jahangir, T. Schimpke, M. Strassburg, K.A. Grossklaus, J.M. Millunchick, and P. Bhattacharya, *IEEE J. Quantum Electron.* 50, 530 (2014).
4. F. Qian, Y. Li, S. Gradečak, H.-G. Park, Y. Dong, Y. Ding, Z.L. Wang, and C.M. Lieber, *Nat. Mater.* 7, 701 (2008).
5. A. Hazari, A. Aiello, T.-K. Ng, B.S. Ooi, and P. Bhattacharya, *Appl. Phys. Lett.* 107, 191107 (2015).
6. A. Hazari, M. Zunaid Baten, L. Yan, J.M. Millunchick, and P. Bhattacharya, *Appl. Phys. Lett.* 109, 191102 (2016).
7. Y.-L. Chang, J.L. Wang, F. Li, and Z. Mi, *Appl. Phys. Lett.* 96, 013106 (2010).
8. H.P.T. Nguyen, S. Zhang, K. Cui, X. Han, S. Fathololoumi, M. Couillard, G.A. Botton, and Z. Mi, *Nano Lett.* 11, 1919 (2011).
9. T. Kehagias, G.P. Dimitrakopulos, P. Becker, J. Kioseoglou, F. Furtmayr, T. Koukoula, and I. Häusler, et al., *Nanotechnology* 24, 435702 (2013).
10. W. Guo, A. Banerjee, P. Bhattacharya, and B.S. Ooi, *Appl. Phys. Lett.* 98, 193102 (2011).
11. S. Deshpande, T. Frost, L. Yan, S. Jahangir, A. Hazari, X. Liu, J. Mirecki-Millunchick, Z. Mi, and P. Bhattacharya, *Nano Lett.* 15, 1647 (2015).
12. J. Tersoff and F.K. LeGoues, *Phys. Rev. Lett.* 72, 3570 (1994).
13. S. Deshpande, J. Heo, A. Das, and P. Bhattacharya, *Nat. Commun.* 4, 1675 (2013).
14. Ž. Gačević, N. Vukmirović, N. García-Lepetit, A. Torres-Pardo, M. Müller, S. Metzner, and S. Albert, et al., *Phys. Rev. B* 93, 125436 (2016).
15. T. Wang, *Semicond. Sci. Technol.* 31, 093003 (2016).
16. P. Wang, Y. Yuan, C. Zhao, X. Wang, X. Zheng, X. Rong, and T. Wang, et al., *Nano Lett.* 16, 1328 (2016).
17. S. Fernández-Garrido, J. Grandal, E. Calleja, M.A. Sánchez-García, and D. López-Romero, *J. Appl. Phys.* 106, 126102 (2009).
18. J. Grandal, M.A. Sánchez-García, E. Calleja, E. Luna, and A. Trampert, *Appl. Phys. Lett.* 91, 021902 (2007).
19. X. Zhang, H. Lourenço-Martins, S. Meuret, M. Kociak, B. Haas, J.-L. Rouvière, P.-H. Jouneau, C. Bougerol, T. Auzelle, D. Jalabert, X. Biquard, B. Gayral, and B. Daudin, *Nanotechnology* 27, 195704 (2016).
20. H.P. Nguyen, M.D. Trung, K. Cui, and Z. Mi, *Nanotechnology* 23, 194012 (2012).
21. L. Yan, S. Jahangir, S.A. Wight, B. Nikoobakht, P. Bhattacharya, and J.M. Millunchick, *Nano Lett.* 15, 1535 (2015).
22. N.V. Sibirev, M. Tchernycheva, M.A. Timofeeva, J.-C. Harmand, G.E. Cirlin, and V.G. Dubrovskii, *J. Appl. Phys.* 111, 104317 (2012).
23. M.J. Bierman, Y.K. Albert Lau, A.V. Kvit, A.L. Schmitt, and S. Jin, *Science* 320, 1060 (2008).
24. Y.P. Varshni, *Physica* 34, 149 (1967).
25. A. Bell, S. Srinivasan, C. Plumlee, H. Omiya, F.A. Ponce, J. Christen, S. Tanaka, A. Fujioka, and Y. Nakagawa, *J. Appl. Phys.* 95, 4670 (2004).
26. B.J. Skromme, J. Jayapalan, R.P. Vaudo, and V.M. Phanse, *Appl. Phys. Lett.* 74, 2358 (1999).